Experimental and Theoretical Characterization of the 2(2)A '-1(2)A ' Transition of BeOH/D

ARTICLE *in* THE JOURNAL OF PHYSICAL CHEMISTRY A · SEPTEMBER 2013

Impact Factor: 2.69 · DOI: 10.1021/jp407655h · Source: PubMed

THE JOURNAL OF PHYSICAL CHEMISTRY A

Article

pubs.acs.org/JPCA

Experimental and Theoretical Characterization of the $2^2A'-1^2A'$ Transition of BeOH/D

Kyle J. Mascaritolo, Jeremy M. Merritt,[†] and Michael C. Heaven*

Department of Chemistry, Emory University, Atlanta, Georgia 30322, United States

Per Jensen

Physikalische und Theoretische Chemie, Bergische Universität Wuppertal, Gaussstrasse 20, D-42097 Wuppertal, Germany

ABSTRACT: The hydroxides of Ca, Sr, and Ba are known to be linear molecules, while MgOH is quasilinear. High-level ab initio calculations for BeOH predict a bent equilibrium structure with a bond angle of 140.9°, indicating a significant contribution of covalency to the bonding. However, experimental confirmation of the bent structure is lacking. In the present study, we have used laser excitation techniques to observe the $2^2A'-1^2A'$ transition of BeOH/D in the energy range of 30300−32800 cm^{-1}. Rotationally resolved spectra were obtained, with sufficient resolution to reveal spin splittings for the electronically excited state. Two-color photoionization was used to determine an ionization energy of 66425(10) cm^{-1}. Ab initio calculations were used to guide the analysis of the spectroscopic data. Multireference configuration interaction calculations were used to construct potential energy surfaces for the $1^2A'$, $2^2A'$, and $1^2A''$ states. The rovibronic eigenstates supported by these surfaces were determined using the Morse oscillator rigid bender internal dynamics Hamiltonian. The theoretical results were in sufficiently good agreement with the experimental data to permit unambiguous assignment. It was confirmed that the equilibrium geometry of the ground state is bent and that the barrier to linearity lies below the zero-point energies for both BeOH and BeOD.

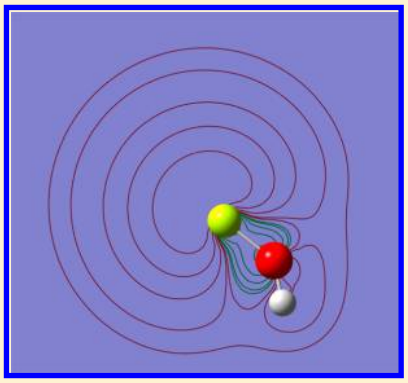

INTRODUCTION

The monohydroxides of the alkaline earth metals (MOH, M = Be, Mg, Ca, Sr, Ba) have been the subject of numerous theoretical[1−11] and experimental studies.[12−26] One of the motivations for this work has been the question of how the M−O bonding changes as a function of the atomic number of the metal. Theoretical studies[1,11] indicate that the heavier members of the group, M = Ca, Sr and Ba, have ionic bonds that are formally M^+-OH^-. This results in a linear equilibrium geometry, as observed for the alkali metal hydroxides.[1] The M^+-OH^- partial charge separation becomes more difficult to accomplish for the lighter alkaline earth metals Be and Mg due to their higher ionization energies (in eV units, 9.323 (Be), 7.646 (Mg), 6.113 (Ca), 5.965 (Sr), and 5.212 (Ba)).[27] Electronic structure calculations indicate that the bonding in BeOH and MgOH has significant contributions from covalent interactions that favor bent geometries.[1,3,4,6] In the case of MgOH, the interplay between ionic and covalent forces results in a potential energy surface that has a linear equilibrium structure but is almost flat with respect to angular displacement near the minimum.[18]

High-level electronic structure calculations have consistently predicted bent equilibrium structures for BeOH, with low barriers to linearity.[1,6,8] For example, the RCCSD(T) calculations of Koput and Peterson,[6] performed using a basis set of 5-ζ quality, yielded an equilibrium bond angle of 140.9°, with a barrier to linearity of 136 cm^{-1}. Unfortunately, the existing experimental data could not be used to determine the geometry. The earliest spectroscopic observations of BeOH were obtained for samples isolated in cryogenic rare gas matrixes. Brom and Weltner[16] recorded the ESR spectrum and concluded that the molecule was most probably linear. Thompson and Andrews[28] trapped the products resulting from the laser ablation of Be in the presence of H_2O. An IR absorption band at 1245.5 cm^{-1} was tentatively assigned to BeOH, but this did not provide any insight concerning the bond angle. Gas-phase emission spectra (300−332 nm) for BeOH and BeOD were reported by Antic-Jovanovic et al.[12] Chemical evidence was used to identify the carrier of the band systems, but there was no attempt to assign the highly congested structure. More recently, electronic spectra for jet-cooled BeOH were obtained by Heaven et al.[29] Partially resolved rotational structure was observed, yielding a first estimate for the ground-state rotational constant. The result was in agreement with the predictions of the highest-level theoretical calculations, but the bands that might be used to probe the question of the bond angle were not identified.

Special Issue: Terry A. Miller Festschrift

Received: July 31, 2013
Revised: September 13, 2013
Published: September 13, 2013

The group IIa MOH species all exhibit allowed electronic transitions that can be approximately described as metal-centered np ← ns electron promotions. The lowest-energy state arising from this excited configuration is of $^2\Pi$ symmetry for the linear geometry. The orbital degeneracy of this state is broken when the molecule is bent, resulting in states of $^2A'$ and $^2A''$ symmetry. For Ca, Sr, and Ba, the states separate upon bending, but both retain the linear equilibrium structure.[19,26,30−32] Spectra for MgOH[17] show that the $2^2A'$ state has a bent equilibrium structure ($\theta_e \approx 119°$) and a barrier to linearity of 1970 cm^{-1}. Theoretical calculations[8] also predict a bent structure for the $1^2A''$ state. As would be expected from these trends, calculations for BeOH predict that both the $2^2A'$ and $1^2A''$ states will have bent equilibrium geometries. The calculations of Theodorakopoulos et al.[8] yielded an approximate barrier to linearity for the $2^2A'$ state of 3710 cm^{-1}.

In the present study, we have examined the $2^2A'-1^2A'$ transitions of BeOH and BeOD using laser excitation techniques. Jet-cooling was used to minimize the spectral congestion. Laser-induced fluorescence (LIF) measurements provided the best resolution, while resonantly enhanced multiphoton ionization (REMPI) with mass-resolved ion detection was used to confirm the attribution of bands to BeOH or BeOD. A two-color ionization technique was used to determine the ionization energy (IE) of BeOH.

Theoretical calculations were carried out to guide the interpretation of the spectra. New potential energy surfaces for the $1^2A'$, $2^2A'$, and $1^2A''$ states were constructed using a multireference configuration interaction method. The rovibronic eigenstates of the surfaces were calculated, and detailed comparisons with the spectroscopic data are reported.

EXPERIMENTAL SECTION

The apparatus used for these experiments has been described in detail previously.[33,34] Gas-phase samples of BeOH/D were generated by pulsed laser ablation. The output of a pulsed Nd/YAG laser (Continuum Minilite II, operating at ∼20 mJ per pulse at 1064 nm) was focused onto the surface of a beryllium rod, which was continuously rotated and translated to expose a fresh surface to each laser shot. The hot plasma produced by the laser vaporization was entrained in a pulse of high-pressure helium carrier gas, which was then expanded as a free jet. To promote the formation of BeOH, HNO_3 vapor was added to the He by passing the carrier gas over the surface of nitric acid. Deuterated nitric acid was used for synthesis of BeOD. The gas pulse was produced by a Jordan valve (0.5 mm orifice diameter) that was operated at source pressures over the range of 20−65 psia, with a pulse duration of 60 μs.

LIF, REMPI, and photoionization efficiency (PIE) spectra were recorded to investigate the electronic structure and bonding of BeOH/D. LIF spectra were recorded with the excitation laser beam positioned 7.5 cm downstream from the nozzle orifice. For the recording of REMPI spectra and PIE curves, the core of the expansion was sampled by a 5 mm diameter skimmer into a differentially pumped chamber that housed a time-of-flight mass spectrometer. A two-color excitation scheme was used to record REMPI spectra with mass-resolved ion detection. The ionizing photon was provided by a KrF laser operating at 248 nm (Lambda Physik Compex 102). The counterpropagating laser beams were overlapped in time and space in the ionization region of the time-of-flight mass spectrometer, along an axis perpendicular to both the molecular beam and the flight tube of the mass spectrometer.

PIE curves were recorded using two tunable dye lasers in order to locate the IE. The first dye laser was set to excite a particular resonant transition of BeOH, while the second dye laser was scanned to locate the onset of ionization, registered by the mass-resolved detection of $BeOH^+$ ions.

The tunable lasers used for these measurements consisted of a Nd/YAG-pumped system (frequency-doubled Continuum 7010 Nd/YAG with a Quanta Ray PDL1e dye laser) and an excimer-pumped dye laser (Lambda Physik Lextra pumping a FL3001 dye laser). Both dye lasers, operated without intracavity etalons, yielded fundamental line widths close to 0.3 cm^{-1} (fwhm). For a few measurements, an etalon was used to reduce the line width of the Lambda Physik laser to approximately 0.06 cm^{-1}. Frequency doubling of the outputs from both dye lasers was used to generate tunable light in the near-UV spectral range. Several laser dyes were used to record the spectra, and the intensities were not corrected for variations in the laser powers. Absolute wavelength calibration of the dye laser fundamentals was provided by a Bristol Instruments wavemeter (model 821) and the simultaneous recording of the I_2 B-X LIF spectrum.[35]

THEORETICAL CALCULATIONS

Potential energy surfaces for the three lowest energy electronic states of BeOH were generated using ab initio electronic structure methods. The MOLPRO 2010.1 suite of programs[36] was used for these calculations. Roos atomic natural orbital basis sets[37] were used for Be, O, and H ((14s, 9p, 4d, 3f) contracted to [5s, 4p, 3d, 2f] for Be and O, (8s, 4p, 3d)/[4s, 3p, 2d] for H). State-averaged complete active space self-consistent field (sa-CASSCF) calculations were carried out for 13 electrons distributed among 11 valence orbitals. The Cartesian axes were chosen with the molecule in the $y-z$ plane, such that z corresponds to the inertial a-axis. To ensure a smooth transition from linear to bent geometries, the calculations did not employ symmetry (C_1 point group). We found that calculations performed using C_s symmetry yielded a larger artificial splitting between the A′ and A″ components of the $\tilde{A}^2\Pi$ state for the linear geometry. Trial calculations were performed with the first four orbitals (O1s, Be1s, O2s, and $O2p_z$ + H1s) constrained to be doubly occupied, leaving an active space of five electrons in seven orbitals (5e/7o; 490 configuration state functions, with active orbital leading contributions of $O2p_y$, $O2p_x$, Be2s − $O2p_z$ + H1s, $Be2p_y$ + H1s − $O2p_y$, $Be2p_x$ − $O2p_x$, $Be2p_z$ + H1s, $Be2p_z$ − H1s + $O2p_z$). The sa-CASSCF results were subsequently used as the starting point for multireference configuration interaction[38,39] calculations that included the Davidson correction[40] (MRCI +Q). In the following, we denote this treatment as sa-CASSCF-MRCI+Q. As the 5e/7o active space proved to be computationally demanding for the generation of a sufficiently fine grid of single-point energies, we examined the consequence of reducing the active space to 3 electrons in 6 orbitals (70 configuration state functions). Within the range of coordinate space that was relevant to the present study, the effect of reducing the active space was marginal. Consequently, the potential energy surfaces were generated using the 3e/6o active space, with all electrons correlated in the MRCI step. The highest-energy molecular orbital held closed in this scheme (orbital 5) was predominantly composed of the in-plane $O2p_y$, with small contributions from Be2s, O2s, and H1s. As a point of comparison, previous sa-CASSCF-MRCI calculations yielded excitation energies for the first excited state of 3.92 (adiabatic

for the linear geometry[8]) and 3.96 eV (vertical[10]), while the present calculations yielded 3.89 eV (adiabatic).

The singly occupied molecular orbital (SOMO) for the ground state is mostly Be 2s, while the $2^2A'$ and $1^2A''$ states are the Renner−Teller split components of a $^2\Pi$ state for the linear geometry. The SOMOs for the latter are predominantly Be2p_y + H1s − O2p_y and Be2p_x − O2p_x. To facilitate modeling for the excited-state rovibronic structure, the spin−orbit coupling constant was calculated for the $^2\Pi$ state with R_{H-O} = 0.95 and R_{O-Be} = 1.40 Å by diagonalization of the matrix for the Breit−Pauli Hamiltonian.[41] The spin−orbit matrix elements were evaluated using the CASSCF wave functions for the $\tilde{X}^2\Sigma^+$, $\tilde{A}^2\Pi(A')$, and $\tilde{A}^2\Pi(A'')$ states (6 × 6 matrix). This yielded a value for A_{SO} of 13.4 cm^{-1}. Note that the value is greater than that of $Be^+(2p)$ (A_{SO} = 4.38 cm^{-1})[42] due to mixing with the O2pπ orbitals.

Equilibrium structures for the ground state $1^2A'$ and the first two excited states, $2^2A'$ and $1^2A''$, are listed in Table 1. Two-

Table 1. Calculated Stationary Points for the Potential Energy Surfaces of BeOH

	$1^2A'$	$2^2A'$	$1^2A''$
R_{O-H}(Å)	0.944	0.948	0.943
R_{Be-O}(Å)	1.401	1.446	1.434
θ (degrees)	139.0	118.2	133.4
barrier (cm^{-1})[a]	262	2322	129

[a]Energy below the minimum-energy linear structure.

dimensional cuts through the potential energy surfaces were produced with the H−O distance held at 0.95 Å. Single-point energies were calculated on a grid with the bond angle (θ) varied from 80 to 180°, in 10° steps. The O−Be bond length was varied from 1.20 to 1.78 Å in 0.02 Å steps. This combination yielded a grid of 330 coordinate points. Calculations were also carried out for variation of R_{H-O} (0.86−1.05 Å in 0.01 Å steps) and θ (125−150° in 5° steps) with R_{Be-O} held at 1.40 Å. Variation of the R_{H-O} distance, over the range sampled by the zero-point motion, resulted in minor changes in the dependencies of the surfaces on R_{O-Be} and θ.

Two-dimensional cuts through the potential energy surfaces for R_{H-O} = 0.95 Å are shown in Figures 1 and 2. The ground-state surface (Figure 1) corresponds to a bent equilibrium structure with a barrier to linearity of 262 cm^{-1}. In comparison

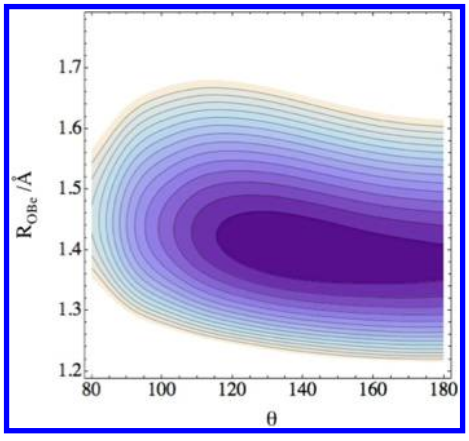

Figure 1. Potential energy contour plot for the $1^2A'$ state of BeOH (R_{HO} = 0.95 Å). The contour lines are drawn at 400 cm^{-1} intervals.

to the ground state, the $2^2A'$ state has a much higher barrier to linearity and a more strongly bent equilibrium structure.

The rovibronic eigenstates of the three potential energy surfaces were calculated using the programs MORBID[43,44] ($1^2A'$) and RENNER[45−47] ($2^2A'$ and $1^2A''$). The analytical potential energy expressions used by these programs are defined in refs 18 and 47. Nonlinear least-squares fits to the single-point energies were used to determine the potential function expansion coefficients. As the data obtained in the experimental part of this study mostly characterize the electronically excited state, we provide the coefficients for the $2^2A'$ and $1^2A''$ state surfaces in Table 2. The standard deviation for the simultaneous fit to all 660 points of the two surfaces was 33 cm^{-1}.

Calculations for the ground state yielded a pattern of energy levels that was similar to that obtained by Koput and Peterson.[6] Here, we label the H−O stretch, the bend, and the O−Be stretch using the quantum number labels ν_1, ν_2, and ν_3. As the molecule executes a large-amplitude bend in this state, the levels are approximately equivalent to those of a linear molecule. The fundamental vibrational intervals for the H−O and O−Be stretches were 3975 and 1267 cm^{-1}, respectively (2931 and 1251 cm^{-1} for BeOD). Excitation of the bending mode (ν_2 = 1) yields a state with a projection of the angular momentum along the a-axis of ±1 (denoted by the unsigned quantum number K_a in the following). This state was at 90 (BeOH) and 50 cm^{-1} (BeOD). These values were somewhat lower than Koput and Peterson's[6] predictions of 100 and 58 cm^{-1}. Zero-point energies from the MORBID calculations were 2836 (BeOH) and 2246 cm^{-1} (BeOD).

To facilitate discussion of the rotational structure, we define N as the quantum number for angular momentum, exclusive of electron and nuclear spin. The total angular momentum, $\vec{J}$ (exclusive of nuclear spin), is given by the vector sum of $\vec{N}$ and the electron spin, $\vec{S}$.

The levels with $J = N + 1/2$ and $J = N - 1/2$ are labeled as $F_1(J)$ and $F_2(J)$, respectively. Our analysis of the predicted rotational structure pertains to levels with N = 0−5 as this was the range observed for jet-cooled BeOH/D. Spin−rotation coupling was not included in the model, and the rotational structure for the zero-point level was well represented by the expression

$$E_{rot}(N) = \bar{B}N(N+1) \quad (1)$$

with $\bar{B}$ (formally $(B + C)/2$) values of 1.2948 (BeOH) and 1.1553 cm^{-1} (BeOD). The effective Hamiltonian for a near-prolate asymmetric rotor

$$\hat{H}_{AR} = A\hat{N}_a^2 + \bar{B}(\hat{N}^2 - \hat{N}_a^2) + \frac{\delta B}{4}(\hat{N}_+^2 + \hat{N}_-^2) \quad (2)$$

where $\delta B = (B - C)$ was used as a model to parametrize the ν_2 = 1 levels. The eigenvalues of eq 2 were obtained using the spectral simulation program PGOPHER.[48] The energy levels predicted by the MORBID calculations were consistent with the $\bar{B}$ constants given above and values for δB of 0.045 (BeOH) and 0.060 cm^{-1} (BeOD). The energies of the ν_2 = 1, N = 1 levels were reproduced using values for the A constants of 89.0 (BeOH) and 48.9 (BeOD) cm^{-1}. It is important to recognize that these ground-state A constants are fitting parameters that are useful for comparison to experimental data. They do not provide a well-defined reflection of simple physical properties such as the bending frequency or the a-axis moment of inertia but are influenced by both.

dx.doi.org/10.1021/jp407655h | J. Phys. Chem. A 2013, 117, 13654−13663

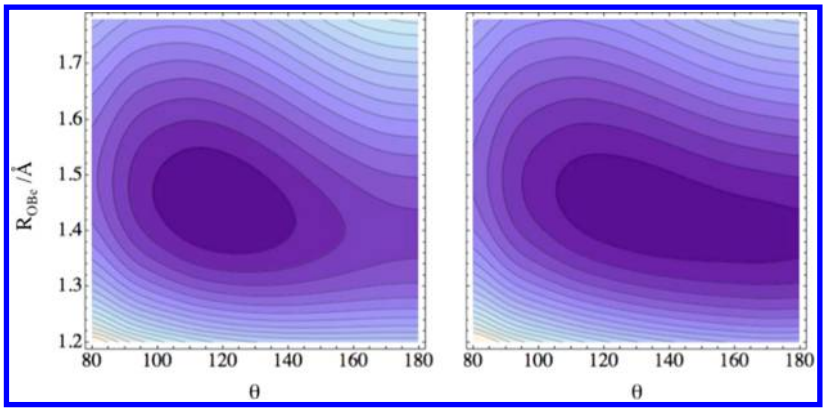

Figure 2. Potential energy contour plots for the $2^2A'$ (left) and $1^2A''$ (right) states of BeOH (R_{HO} = 0.95 Å). The contour lines are drawn at 1000 cm^{-1} intervals, relative to the minimum of the $2^2A'$ state. The lowest-energy contour line of the $1^2A'$ surface corresponds to 3000 cm^{-1}.

Table 2. Potential Energy Surface Expansion Coefficients for the $2^2A'$ and $1^2A''$ States of BeOH[a]

$R_{HO}^{(ref)}$/Å	0.936914	$R_{OBc}^{(ref)}$/Å	1.393966
a_1/Å^{-1}	2.20	a_3/Å^{-1}	1.76
f_{11}	52616.506	f_{33}	47146.401
f_{111}	−442.11135	f_{333}	−115.38494

	A′ surface	A″ surface
$f_0^{(1)}$	−9929.3062	−3002.7012
$f_0^{(2)}$	11785.571	9020.317
$f_0^{(3)}$	−2465.1859	−6532.0545
$f_0^{(4)}$	1205.8996	3998.4399

	A′ surface	A″ surface		A′ surface	A″ surface
$f_1^{(1)}$	−6549.6897	−3921.3821	$f_3^{(1)}$	−20229.524	−23422.812
$f_1^{(2)}$	3330.3246	−2387.789	$f_3^{(2)}$	7955.0694	11422.061
$f_1^{(3)}$	0	0	$f_3^{(3)}$	409.95981	−796.38732
$f_1^{(4)}$	0	0	$f_3^{(4)}$	−1459.6534	−1413.1003
$f_{11}^{(1)}$	−14883.412	1285.3227	$f_{33}^{(1)}$	5058.5048	−6764.3697
$f_{11}^{(2)}$	15469.468	−12006.303	$f_{33}^{(2)}$	−5470.9831	12966.755
$f_{11}^{(3)}$	0	0	$f_{33}^{(3)}$	542.46579	−7456.1833
$f_{111}^{(1)}$	0	0	$f_{333}^{(1)}$	−873.0604	−2868.671
$f_{111}^{(2)}$	0	0	$f_{333}^{(2)}$	768.59156	1343.1058

[a]Parameters are in cm^{-1} unless otherwise specified. The coefficients are defined in ref 47.

Table 3. Calculated and Fitted Rotational Energy Levels of the $2^2A'$ (0,0,0) State of BeOH[a]

N	$F_1(A')$	$F_1(A'')$	$F_2(A')$	$F_2(A'')$
		K_a = 0		
0			0.00	
1		2.51 (2.50)		2.51 (2.50)
2	7.54 (7.50)		7.54 (7.50)	
3		15.08 (15.01)		15.08 (15.01)
4	25.13 (25.01)		25.13 (25.01)	
		K_a = 1		
1	28.41 (27.39)	28.36 (27.35)	27.91 (27.01)	27.85 (26.97)
2	33.27 (32.40)	33.44 (32.54)	33.01 (32.06)	33.19 (32.21)
3	41.04 (39.96)	40.69 (39.67)	40.86 (39.82)	40.52 (39.54)
4	50.61 (49.57)	51.19 (50.05)	50.47 (49.46)	51.05 (49.94)
		K_a = 2		
2	110.28 (106.82)	110.28 (106.82)	109.19 (105.98)	109.19 (105.98)
3	117.70 (114.24)	117.70 (114.24)	116.98 (113.68)	116.98 (113.68)
4	127.67 (124.20)	127.67 (124.20)	127.13 (123.77)	127.13 (123.77)

[a]Energies are in cm^{-1}. The numbers in parentheses were generated from fitted molecular constants. See the text for details.

The potential energy surface for the $2^2A'$ surface has a substantial barrier to linearity, such that the lower-energy vibrational levels can be described in terms of a bent molecule model. The fundamental vibrational intervals were predicted to be 3842, 782, and 1182 cm^{-1} (BeOH, zero-point energy = 2993 cm^{-1}) and 2835, 600, and 1156 cm^{-1} (BeOD, zero-point

dx.doi.org/10.1021/jp407655h | J. Phys. Chem. A 2013, 117, 13654−13663

energy = 2349 cm^{-1}). The RENNER calculations included spin−orbit coupling using a single value of 13.4 cm^{-1} for the coupling constant. As for the ground state, spin−rotation interactions were not included. The spectroscopic data included transitions that accessed excited-state K_a = 0, 1, and 2 levels. Predicted rotational energies for the $2^2A'$ (0,0,0) levels of BeOH and BeOD are presented in Tables 3 and 4. The spin−

Table 4. Calculated and Fitted Rotational Energy Levels of the $2^2A'$ (0,0,0) State of BeOD[a]

N	$F_1(A')$	$F_1(A'')$	$F_2(A')$	$F_2(A'')$
		K_a = 0		
0			0.00	
1		2.31 (2.30)		2.31 (2.30)
2	6.92 (6.91)		6.92 (6.91)	
3		13.84 (13.82)		13.84 (13.82)
4	23.05 (23.03)		23.05 (23.03)	
		K_a = 1		
1	16.56 (16.00)	16.47 (15.91)	16.28 (15.81)	16.19 (15.72)
2	20.96 (20.40)	21.23 (20.67)	20.81 (20.31)	21.08 (20.58)
3	28.27 (27.71)	27.72 (27.17)	28.16 (27.64)	27.62 (27.10)
4	36.75 (36.20)	37.66 (37.10)	36.68 (36.15)	37.58 (37.05)
		K_a = 2		
2	63.41 (61.42)	63.41 (61.42)	62.81 (61.01)	62.81 (61.01)
3	70.26 (68.30)	70.26 (68.30)	69.85 (68.02)	69.85 (68.02)
4	79.45 (77.49)	79.45 (77.49)	79.14 (77.28)	79.14 (77.28)

[a]Energies are in cm^{-1}. The numbers in parentheses were generated from fitted molecular constants. See the text for details.

orbit coupling was mostly quenched near the equilibrium bond angle; therefore, the angular momentum coupling was close to the Hund's case b limit. The effective zero-point rotational constants were A = 27.0, $\overline{B}$ = 1.257, δB = 0.05 (BeOH) and A = 15.2, $\overline{B}$ = 1.153, δB = 0.08 cm^{-1} (BeOD). The values for δB were close to those estimated using the equilibrium coordinates (0.060 and 0.090 cm^{-1}).

The energy of the zero-point level of $1^2A''$, relative to that of the $2^2A'$ state, was predicted to be 2103 (BeOH) and 2118 cm^{-1} (BeOD). As this energy range was not accessed in our experiments, we do not describe the energy level characteristics of the $1^2A''$ potential energy surface here.

At the ground-state equilibrium geometry, the sa-CASSCF calculations yielded values for the electric dipole transition moments of $|\langle 2^2A'|\mu_b|1^2A'\rangle| = 3.8$ D and $|\langle 2^2A'|\mu_a|1^2A'\rangle| = 0.14$ D. Hence, the transition is expected to follow b-type selection rules ($\Delta K_a = \pm 1$, $\Delta J = 0, \pm 1$), and the allowed bands originating from cold BeOH/D should correspond to $K_a' = 1 \leftarrow K_a'' = 0$. When this selection rule is taken into account, the calculations described above predict that the lowest-energy feature arising from the zero-point level of the ground state will be at 31532 (BeOH) and 31466 cm^{-1} (BeOD), defining an isotope shift of 66 cm^{-1}.

Here, we correct a misstatement concerning the transition type made in the preliminary discussion of the spectrum by Heaven et al.[29] It was noted that the prominent Q-branches seen in the spectra were indicative of a perpendicular transition (relative to the *a*-axis), which therefore constrained the upper state to be of A″ symmetry. The first part of this assertion was correct, but the symmetry implication is not. As demonstrated below, the Q-branch intensities are consistent with b-type selection rules for a $^2A'-^2A'$ transition.

EXPERIMENTAL RESULTS AND ANALYSES

Figure 3 shows low-resolution survey scans for BeOH and BeOD recorded using REMPI detection. Over the energy range

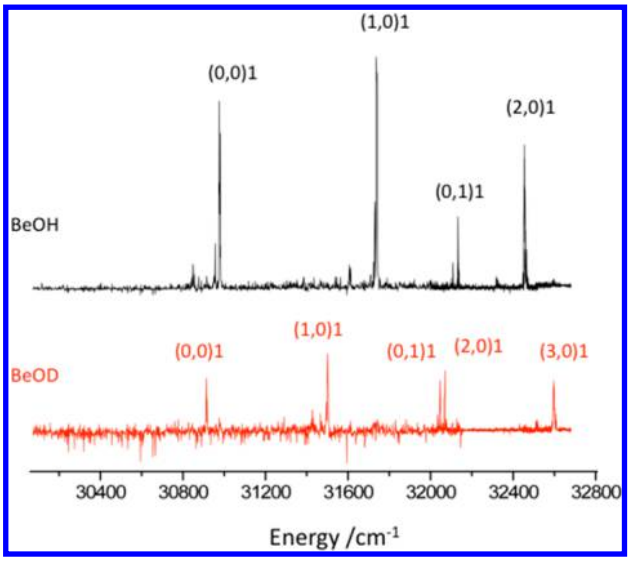

Figure 3. Low-resolution REMPI survey spectra for BeOH and BeOD.

examined (30300−32800 cm^{-1}), the spectra exhibited a dominant vibrational progression with average intervals of 730 (BeOH) and 560 cm^{-1} (BeOD). Weaker features were present, in positions that were consistent with those predicted for the sub-bands associated with the main progression. From the band spacings and the isotope shifts, the main progression could be unambiguously assigned to the bending mode. Transitions involving excitation of the H−O stretch were not observed in this study; therefore, we label the excited-state vibrational levels using the notation $(\nu_2,\nu_3)K_a$.

An expanded scan of the 30840−31015 cm^{-1} region, recorded using LIF, is shown in Figure 4. DNO_3 was used as

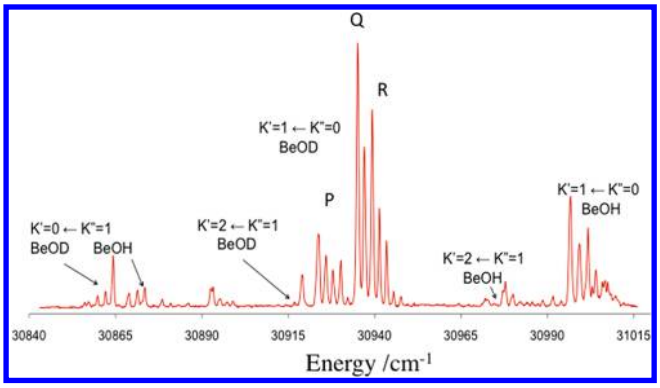

Figure 4. LIF spectrum for a mixture of BeOH and BeOD.

the hydroxyl source for this experiment, but bands of both BeOD and BeOH were clearly present. For these conditions, the bands showed partially resolved rotational structure. The central feature of this trace is the $K_a' = 1 \leftarrow K_a'' = 0$ sub-band of the BeOD origin transition. The P-, Q-, and R-branch structures of this band, along with the relative branch intensities, confirm that this is a $\Delta K_a = +1$ transition. The equivalent band for BeOH can be seen at the high-frequency end of Figure 4. As discussed below, the P-branch regions of

dx.doi.org/10.1021/jp407655h | J. Phys. Chem. A 2013, 117, 13654−13663

the $K_a' = 1 \leftarrow K_a'' = 0$ sub-bands also include additional lines that belong to the $K_a' = 2 \leftarrow K_a'' = 1$ sub-bands. The $\Delta K_a = -1$ transitions arising from $K_a'' = 1$ are also present in this trace, with Q-branch features near 30874 (BeOH) and 30864 cm^{-1} (BeOD). As expected for $\Delta K_a = -1$, the P-branch lines were more intense than those of the R-branch. The first lines of each branch, labeled using the N quantum number, were P(1) and R(1) for the $\Delta K_a = -1$ sub-bands and P(2) and R(0) for the $K_a' = 1 \leftarrow K_a'' = 0$ sub-bands, confirming the K_a assignments.

Higher-resolution spectra for the origin bands were recorded using an intracavity etalon to reduce the laser linewidth. Figures 5 and 6 present the more intense lines of the $K_a' = 1 \leftarrow K_a'' = 0$ sub-bands, where the low-N lines show spin splitting. Modeling of the higher-resolution spectra was carried out using the program PGOPHER.[48] Both the ground and excited states were represented using the rigid near-prolate top Hamiltonian given by eq 2. The spin splitting in the $2^2A'$ state was reproduced by adding the term arising from the a-axis spin−rotation interaction (ε_{aa}).[48,49] Examples of the fitting are shown as the downward-going traces in Figures 5 and 6. All fits were carried out using the least-squares fitting capabilities of PGOPHER.[48] The rotational temperature was set to 8 K. Initial fitting of the $K_a' = 1 \leftarrow K_a'' = 0$ sub-bands was accomplished by varying ν_0 (the band origin), $\bar{B}''$, $\bar{B}'$, and ε_{aa}'. The parameters A', A'', $\delta B'$, and $\delta B''$ were held at the values derived from the theoretical calculations. This yielded fits with standard deviation below 0.05 cm^{-1}. In the next step, data for the $K_a' = 0 \leftarrow K_a'' = 1$ and $K_a' = 2 \leftarrow K_a'' = 1$ sub-bands were included, and all of the parameters listed above were treated as variables. In this model, the spin splittings were determined by ε_{aa}', while the combination defect (displacement of the Q-branch relative to the P- and R-branches) was controlled by $\delta B'$ and $\delta B''$. At this stage, the dependence of $\bar{B}$ on K_a was neglected. For the ground state, this proved to be an acceptable approximation. However, for the BeOH origin, the fits were improved when the excited-state $\bar{B}'$ constant was slightly decreased for $K_a' = 0$.

Due to correlations between the upper and lower state constants, fits where all of the constants were allowed to vary simultaneously were often unstable, yielding physically unreasonable parameter values. Consequently, multiple fits were carried out to systematically refine the constants by freezing out different subgroups. With this approach, the standard deviation for the constants from the constrained fits were artificially low. The uncertainties given in Tables 5−7 were estimated by exploring the range of value choices for a given constant that could be accommodated by physically reasonable adjustments of correlated constants.

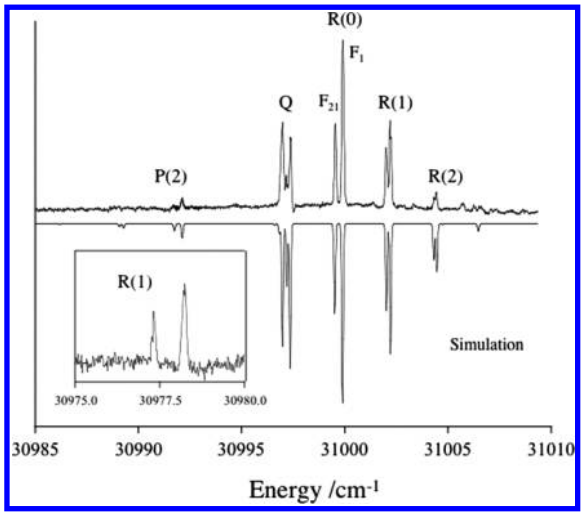

Figure 5. High-resolution LIF spectrum for the origin band of the $2^2A'-1^2A'$ transition of BeOH. The upper trace shows the rotational lines of the $K_a = 1 - K_a = 0$ sub-band, while the inset show the R(1) feature of the $K_a = 2 - K_a = 1$ sub-band. The downward-going trace is a simulation based on the constants given in Tables 5 and 6

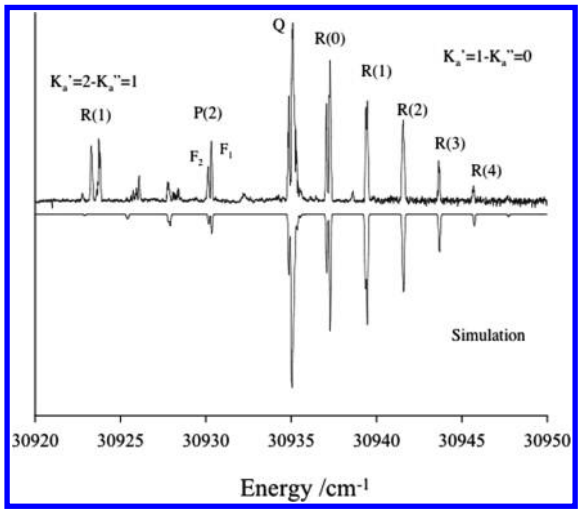

Figure 6. High-resolution LIF spectrum for the origin band of the $2^2A'-1^2A'$ transition of BeOD. The upper trace shows the rotational lines of the $K_a = 1 - K_a = 0$ and 2−1 sub-bands, The downward-going trace is a simulation based on the constants given in Tables 5 and 7

Table 5. Ground-State Properties of BeOH and BeOD

property	BeOH	BeOD	source
A	99.9(1)	57.9(1)	*a*
$\bar{B}$	1.295(4)	1.155(4)	*a*
δB	0.04(2)	0.06(2)	*a*
$E(K_a = 1, N = 1)$	101.2(2)	59.0(2)	*a*
$E(K_a = 1, N = 1)$	99.9	58.1	*b*
$E(K_a = 1, N = 1)$	90.1	49.9	*c*

[a]Experimental values in units of cm^{-1}. [b]Theoretical calculations of Koput and Peterson.[6] [c]Present theoretical calculations.

The best-fit molecular constants for the ground states of BeOH and BeOD, derived from the higher-resolution spectra,

Table 6. Molecular Constants for the $2^2A'$ State of BeOH[a]

$(\nu_2\nu_3)K_a$	ν_0	A	$\bar{B}$	δB	ε_{aa}
(0,0)0	30972.6(1)	26.0(1)	1.251(4)	0.05(1)	0.52(6)
(0,0)1	30972.6(1)	26.0(1)	1.251(4)	0.05(1)	0.52(6)
(0,0)2	30972.6(1)	26.0(1)	1.261(4)	0.05(1)	0.52(6)
(1,0)0	31719.9(2)	30.2(2)	1.260(5)	0.07(2)	0.70(8)
(1,0)1	31719.9(2)	30.2(2)	1.240(5)	0.07(2)	0.70(8)
(1,0)2	31719.9(2)	30.2(2)	1.240(5)	0.07(2)	0.70(8)
(0,1)1	32106.2(2)	27.2(2)	1.257(5)	0.05(2)	0.5(1)
(2,0)0	32425.6(2)	32.3(2)	1.220(5)	0.05(2)	1.7(1)
(2,0)1	32425.6(2)	32.3(2)	1.261(5)	0.05(2)	1.7(1)
(2,0)2	32425.6(2)	32.3(2)	1.261(5)	0.05(2)	1.7(1)

[a]Constants are in units of cm^{-1}.

dx.doi.org/10.1021/jp407655h | J. Phys. Chem. A 2013, 117, 13654−13663

Table 7. Molecular Constants for the $2^2A'$ State of BeOD[a]

$(\nu_2,\nu_3)K_a$	ν_0	A	$\bar{B}$	δB	ε_{aa}
(0,0)0	30921.4(1)	14.7(1)	1.152(4)	0.09(1)	0.25(6)
(0,0)1	30921.4(1)	14.7(1)	1.152(4)	0.09(1)	0.25(6)
(0,0)2	30921.4(1)	14.7(1)	1.152(4)	0.09(1)	0.25(6)
(1,0)0	31499.2(2)	16.8(2)	1.160(5)	0.09(2)	0.25(8)
(1,0)1	31499.2(2)	16.8(2)	1.152(5)	0.09(2)	0.25(8)
(1,0)2	31499.2(2)	16.8(2)	1.152(5)	0.09(2)	0.25(8)
(0,1)0	32038.6(2)	15.4(2)	1.139(5)	0.06(2)	0.25(8)
(0,1)1	32038.6(2)	15.4(2)	1.139(5)	0.06(2)	0.25(8)
(0,1)2	32038.6(2)	15.4(2)	1.139(5)	0.06(2)	0.25(8)
(2,0)0	32058.5(2)	18.5(2)	1.140(5)	0.09(2)	0.25(8)
(2,0)1	32058.5(2)	18.5(2)	1.140(5)	0.09(2)	0.25(8)
(2,0)2	32058.5(2)	18.5(2)	1.140(5)	0.09(2)	0.25(8)
(3,0)1	32572.2(2)	22.1(2)	1.152(5)	0.10(2)	0.25(8)
(3,0)2	32572.2(2)	22.1(2)	1.152(5)	0.10(2)	0.25(8)

[a]Constants are in units of cm^{-1}.

are presented in Table 5. Note the large values for the A'' constants, which are consistent with the present theoretical calculations and those of Koput and Peterson.[6] The observation of transitions from $K_a'' = 1$ indicates that the K_a population distribution was not in thermal equilibrium with the N-based rotational distributions.

The system of $K_a' = 0$, 1, and 2 sub-bands described for the origin was also observed in association with the $\nu_2 = 1$ and 2 levels of BeOH and the $\nu_2 = 1$, 2, and 3 levels of BeOD. In addition, the sub-bands of the $\nu_3 = 1$ O−Be stretch were recorded for both isotopologues. These vibrationally excited levels were recorded at a resolution of 0.5 cm^{-1}, which was sufficient to resolve the rotational lines and partially resolve some of the spin splittings. In fitting these data, the molecular constants for the ground states were held fixed at the values given in Table 5. Excited-state molecular constants are listed in Table 6 for BeOH and Table 7 for BeOD. The band origin (ν_0) values in these tables correspond to the hypothetical $N' = K_a' = 0 \leftarrow N'' = K_a'' = 0$ transitions. Vibrational intervals for the $2^2A'$ state, derived from the ν_0 values, are listed in Table 8.

Table 8. Vibrational Intervals for the $2^2A'$ State of BeOH/D[a]

isotopologue	interval	observed	calculated
BeOH	(1,0)−(0,0)	747.3(3)	782.4
BeOH	(2,0)−(1,0)	705.7(3)	736.3
BeOH	(0,1)−(0,0)	1140.0(3)	1181.9
BeOD	(1,0)−(0,0)	577.8(3)	600.5
BeOD	(2,0)−(1,0)	559.3(3)	573.7
BeOD	(3,0)−(2,0)	513.7(3)	536.1
BeOD	(0,1)−(0,0)	1117.2(3)	1156.5

[a]Energies are in units of cm^{-1}.

The IE of BeOH was determined by recording the two-photon ionization efficiency spectrum. For this measurement, the first laser was tuned to the R(0) line of the $K_a' = 1 \leftarrow K_a'' = 0$ origin band at 30999.5 cm^{-1}. The second laser, which was temporally overlapped with the first, was tuned through the energy range where ionization was expected.[8,10] The result of this scan is shown as the upper trace in Figure 7, where the lowest-energy feature observed is marked with an arrow. The lower trace in Figure 7 was recorded with a delay of 20 ns between the two laser pulses. This was done to check for

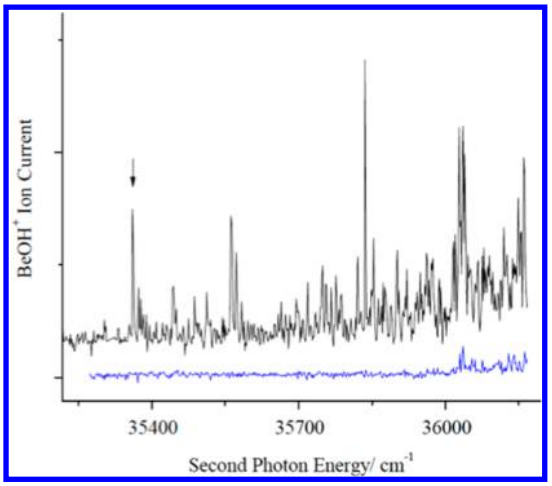

Figure 7. PIE spectrum for BeOH. The first laser was tuned to the R(0) line of the $K_a' = 1 - K_a'' = 0$ band at 30999.5 cm^{-1}.

features that might have arisen from one-color, two-photon ionization. None were detected at the threshold energy. The ionization spectrum shows resolved structure resulting from autoionizing resonances. The first prominent feature, used here to determine the IE, also appears to be a resonance. This spectrum was recorded in an electric field of $F = 145$ V/cm. Correcting the threshold energy for the field, by means of the expression[50] $\Delta E(cm^{-1}) = 6(F(V/cm))^{1/2}$, yielded an IE of 66425 cm^{-1}. Taking into account the uncertainties associated with the determination of the low-energy edge of the first feature, we estimate that the error range for IE is ±10 cm^{-1}.

DISCUSSION

The level of agreement between the theoretically predicted properties of BeOH/D and the near-UV band system was sufficient to achieve unambiguous assignment of the observed rovibronic features. The ground-state $\bar{B}$ constants derived from both the present calculations and those of Koput and Peterson[6] were within the error limits of the values determined from our highest-resolution spectra. The measured intervals between the $K_a'' = 1$ and $K_a'' = 0$ levels were higher than both the predictions of Koput and Peterson[6] and the present calculations, with the former being closer to the experimental values. Although the present calculations yielded a higher barrier to linearity, we found that it was primarily the behavior of the effective bending potential at the outer turning points (smaller values for θ) that determined the K_a'' 1−0 intervals. One-dimensional cuts through the potential energy surfaces showed that the surface of Koput and Peterson[6] was steeper at smaller angles, producing larger spacings. On the basis of this analysis, it seems that the surface generated from the RCCSD(T) calculations of Koput and Peterson[6] is of better quality than that of our CASSCF/MRCI+Q results. This may be attributed to the larger size basis sets used in the former study (up to aug-cc-pV5Z) combined with optimization that was focused on just the ground state. The agreement between the experimental and theoretical results is close enough to confirm that the ground-state zero-point level of BeOH/D is quasilinear.

Our theoretical calculations predicted that the first Q-branch line of the $2^2A'-1^2A'$ origin transition ($K_a' = 1 - K_a'' = 0$ sub-band) would be observed at 31497 (BeOH) and 31443 cm^{-1} (BeOD). These values overestimated the experimental results

dx.doi.org/10.1021/jp407655h | J. Phys. Chem. A 2013, 117, 13654−13663

by 500 and 508 cm^{-1}, which is an acceptable level of agreement for an electronic transition energy of this magnitude. The measured and calculated isotopic shifts (62 versus 54 cm^{-1}, determined using the Q(1) lines) were also in respectable agreement. The adiabatic excitation energy predicted by Theodorakopoulos et al.[8] (31620 cm^{-1}) and the vertical energy of Zaidi et al.[10] (31940 cm^{-1}) are also consistent with the experimental results.

For the zero-point levels of BeOH/D $2^2A'$, comparisons of the observed and predicted rotational energies are presented in Tables 3 and 4. The experimentally determined energies, which are given in parentheses, were generated using the fitted molecular constants from Tables 3 and 4. Energy intervals associated with the $\overline{B}'$ molecular constant were found to be very close to the measured values. The predicted spacings between the $K_a' = 0$, 1, and 2 manifolds were slightly too large. As noted above, BeOH/D can be treated as a bent molecule for levels near the bottom of the $2^2A'$ state. Consequently, the K_a' spacings can be related, via the A rotational constant, to the average bond angle. The calculated A constants were overestimated by an amount that indicated that the vibrationally averaged bond angle of the theoretical calculation was too large by 1.5 (BeOH) and 1.3° (BeOD). The $2^2A'$ state spin splittings were adequately reproduced by the RENNER calculations using $A_{SO} = 13.4$ cm^{-1}.

From Tables 6 and 7, it can be seen that the A constants increased with increasing excitation of the bending mode. This trend was also exhibited by the theoretical calculations, which yielded A constants for $2^2A'$ BeOH(D) of 27.2(15.4), 31.9(17.8), 32.4(19.4), and (22.2) cm^{-1} for $\nu_2 = 0$, 1, 2, and 3. The calculated and measured intervals between successive bending levels and the frequencies for the O−Be stretch fundamental are presented in Table 8. Here, it can be seen that the bending mode was markedly anharmonic. The frequencies of both the bending levels and the O−Be stretch fundamentals were overestimated by the calculations, indicating that the potential energy surface is somewhat too steep for motions along these vibrational coordinates. Despite this shortcoming, the predictions for vibrationally excited levels were close enough to the experimental data to provide the correct ordering for the nearby (0,1) and (2,0) states of BeOD (cf. Figure 3). Assignment of the experimental data for these two bands was based on the behavior of the A constants.

As part of their study of the HBeO isomer, Zaidi et al.[10] reported a vertical excitation energy for BeOH of 31940 cm^{-1} for the $2^2A'-1^2A'$ transition, derived from a large-scale sa-CASSCF/MRCI+Q calculation that included correlation of the Be 1s electrons. The present calculations are in reasonably good agreement with this result, and both are consistent with the experimental observations. Theodorakopoulos et al.[8] carried out a more extensive study of the $2^2A'$ potential energy surfaces. Their equilibrium parameters (determined with R_{H-O} fixed at 0.9435 Å) were $R_{O-Be} = 1.48$ Å and $\theta = 116°$, with a barrier to linearity of 3710 cm^{-1}. Compared with the properties given in Table 1, the smaller bond angle of Theodorakopoulos et al.[8] is in better agreement with the experimentally determined A constants, while the equilibrium bond length provided by the present calculations is in better agreement with the observed $\overline{B}$ constants. The barrier heights predicted by the present calculations and those of Theodorakopoulos et al.[8] are significantly different. As the latter study did not report vibrational energies, it is difficult to know if their potential energy surface is consistent with the spectroscopic data. Although the present calculations yielded a lower energy barrier, the potential surface led to bending frequencies that were too high. Examination of the angular cut through the potential energy surface of Theodorakopoulos et al. (Figure 4 of ref 8) indicate that this surface will also overestimate the bending frequency and that the irregular shape of the curve near 140° may produce erratic vibrational intervals.

Theodorakopoulos et al.[8] estimated the IE of BeOH by considering the energy difference between the minimum-energy linear structures for BeOH and $BeOH^+$. Geometry optimization confirmed the expected linear geometry of the cation. Given the low barrier to linearity for the ground state of BeOH, the IE of the linear molecule should provide a good approximation for the adiabatic IE. The present measurements established an IE of 66425(10) cm^{-1}. Assuming that the zero-point energies of BeOH and $BeOH^+$ are comparable, the calculated value of 65330 cm^{-1} is found to be reasonably accurate.

CONCLUSIONS

Comparison of the spectroscopic data and theoretical calculations for BeOH/D confirms earlier predictions that the molecule is quasilinear in the ground state. The potential energy surface has a bent equilibrium geometry, but the zero-point vibrational level lies well above the barrier to linearity. These findings support the expectation that bonding in BeOH has a greater degree of covalency than is found for any of the other alkaline earth monohydroxides.[1] The ground-state potential energy surface and rovibronic eigenstate calculations of Koput and Peterson[6] were found to be in very good agreement with the experimental data.

The electronic transition observed in this study, $2^2A'-1^2A'$, can be attributed to a mostly Be-centered 2p−2s electron promotion. The $2^2A'$ potential energy surface has a bent equilibrium structure with a moderately high barrier to linearity. As a consequence, the lower-energy rovibronic levels follow the behavior expected for a bent molecule. Theoretical calculations were used to predict the potential energy surface and the rovibronic eigenstates of the $2^2A'$ state. The results were in respectable agreement with the spectroscopic data, and the characteristics of the surface were broadly in agreement with the results from a previously published MRCI calculation.[8] The favorable comparison indicates that the low-lying electronically excited states of BeOH can be predicted with a useful level of confidence using multireference electronic structure techniques.

AUTHOR INFORMATION

Corresponding Author

*E-mail: mheaven@emory.edu. Phone: 404 727 6617. Fax: 404 727 6586.

Present Address

†J.M.M.: Eli Lilly and Co., Chemical Product R&D, Lilly Technology Center South, Indianapolis, IN 46221. E-mail: merrittje@lilly.com.

Notes

The authors declare no competing financial interest.

ACKNOWLEDGMENTS

The work conducted at Emory University was supported by the NSF under Grant CHE-0956442. The electronic structure calculations reported here were carried out using the resources of the Cherry Emerson Center for Scientific Computation,

which is supported by the NSF MRI-R2 Grant CHE-0958205. The work of P.J. is supported in part by the Deutsche Forschungsgemeinschaft and the Fonds der Chemischen Industrie

REFERENCES

(1) Bauschlicher, C. W., Jr.; Langhoff, S. R.; Partridge, H. Ab Initio Study of the Alkali and Alkaline-Earth Monohydroxides. *J. Chem. Phys.* **1986**, *84*, 901−909.

(2) Bauschlicher, C. W., Jr.; Langhoff, S. R.; Steimle, T. C.; Shirley, J. E. The Permanent Electric Dipole Moment of Calcium Hydroxide (CaOH). *J. Chem. Phys.* **1990**, *93*, 4179−4186.

(3) Hinchliffe, A. Structure and Electronic Properties of the Radicals BeOH and MgOH. *J. Mol. Struct.* **1980**, *64*, 289−292.

(4) Koput, J.; Carter, S.; Peterson, K. A.; Theodorakopoulos, G. The Ab Initio Potential Energy Surface and Vibrational−Rotational Energy Levels of $X^2\Sigma^+$ MgOH. *J. Chem. Phys.* **2002**, *117*, 1529−1535.

(5) Koput, J.; Peterson, K. A. Ab Initio Potential Energy Surface and Vibrational−Rotational Energy Levels of $X^2\Sigma^+$ CaOH. *J. Phys. Chem. A* **2002**, *106*, 9595−9599.

(6) Koput, J.; Peterson, K. A. Ab Initio Prediction of the Potential Energy Surface and Vibrational−Rotational Energy Levels of X^2A' BeOH. *J. Phys. Chem. A* **2003**, *107*, 3981−3986.

(7) Palke, W. E.; Kirtman, B. Calculations of the Bending Potentials of Magnesium Hydroxide (MgOH) and Beryllium Hydroxide (BeOH). *Chem. Phys. Lett.* **1985**, *117*, 424−426.

(8) Theodorakopoulos, G.; Petsalakis, I. D.; Hamilton, I. P. Ab Initio Calculations on the Ground and Excited States of BeOH and MgOH. *J. Chem. Phys.* **1999**, *111*, 10484−10490.

(9) Theodorakopoulos, G.; Petsalakis, I. D.; Liebermann, H.-P.; Buenker, R. J.; Koput, J. Ab Initio Calculations on Electronic States of CaOH. *J. Chem. Phys.* **2002**, *117*, 4810−4819.

(10) Zaidi, A.; Lahmar, S.; Ben Lakhdar, Z.; Rosmus, P.; Chambaud, G. Theoretical Study of HBeO. *Chem. Phys.* **2006**, *321*, 41−47.

(11) Vasiliu, M.; Feller, D.; Gole, J. L.; Dixon, D. A. Structures and Heats of Formation of Simple Alkaline Earth Metal Compounds: Fluorides, Chlorides, Oxides, and Hydroxides for Be, Mg, and Ca. *J. Phys. Chem. A* **2010**, *114*, 9349−9358.

(12) Antic-Jovanovic, A.; Bojovic, V.; Pesic, D. Electronic Bands of Beryllium Hydroxide (BeOH and BeOD). *Spectrosc. Lett.* **1988**, *21*, 757−765.

(13) Ziurys, L. M.; Fletcher, D. A.; Anderson, M. A.; Barclay, W. L., Jr. Rest Frequencies for Alkaline Earth Hydroxide Radicals ($X^2\Sigma^+$). *Astrophys. J., Suppl. Ser.* **1996**, *102*, 425−434.

(14) Fletcher, D. A.; Anderson, M. A.; Barclay, W. L., Jr.; Ziurys, L. M. Millimeter-Wave Spectroscopy of Vibrationally Excited Ground State Alkaline-Earth Hydroxide Radicals ($X^2\Sigma^+$). *J. Chem. Phys.* **1995**, *102*, 4334−4339.

(15) Brom, J. M., Jr.; Weltner, W., Jr. ESR Spectrum and Structure of the Magnesium Hydroxide Radical. *J. Chem. Phys.* **1973**, *58*, 5322−5330.

(16) Brom, J. M., Jr.; Weltner, W., Jr. ESR Spectrum of the Beryllium Hydroxide (BeOH) Molecule. *J. Chem. Phys.* **1976**, *64*, 3894−3895.

(17) Ni, Y. *Laser Spectroscopy and Structure of Magnesium Hydroxide and Deuterated Magnesium Hydroxide: The A−X System*. Ph.D. Thesis, University of California, Santa Barbara: Santa Barbara, CA, 1986; p 127.

(18) Bunker, P. R.; Kolbuszewski, M.; Jensen, P.; Brumm, M.; Anderson, M. A.; Barclay, W. L., Jr.; Ziurys, L. M.; Ni, Y.; Harris, D. O. New Rovibrational Data for MgOH and MgOD and the Internuclear Potential Function of the Ground Electronic State. *Chem. Phys. Lett.* **1995**, *239*, 217−222.

(19) Tandy, J. D.; Wang, J. G.; Bernath, P. F. High-Resolution Laser Spectroscopy of BaOH and BaOD: Anomalous Spin−Orbit Coupling in the $A^2\Pi$ State. *J. Mol. Spectrosc.* **2009**, *255*, 63−67.

(20) Wang, J. G.; Dick, M. J.; Sheridan, P. M.; Yu, S.; Bernath, P. F. Further Spectroscopic Investigations of the High Energy Electronic States of SrOH: The $B'^2\Sigma^+(0\,0\,0)-A^2\Pi(0\,0\,0)$ and the $D^2\Sigma^+(0\,0\,0)-A^2\Pi(0\,0\,0)$ Transitions. *J. Mol. Spectrosc.* **2007**, *245*, 26−33.

(21) Beardah, M. S.; Ellis, A. M. Observation of a New $^2\Sigma^+-^2\Sigma^+$ Transition of the SrOH Free Radical. *J. Mol. Spectrosc.* **2003**, *218*, 80−84.

(22) Li, M.; Coxon, J. A. Dye Laser Excitation Studies of the $A^2\Pi(100)/(020)-X^2\Sigma^+(020)/(000)$ Bands of CaOD: Analysis of the $A^2\Pi(100)/(020)$ Fermi Resonance. *J. Chem. Phys.* **1996**, *104*, 4961−4977.

(23) Presunka, P. I.; Coxon, J. A. Laser Excitation and Dispersed Fluorescence Investigations of the $\tilde{A}^2\Pi-\tilde{X}^2\Sigma^+$ System of SrOH. *Chem. Phys.* **1995**, *190*, 97−111.

(24) Anderson, M. A.; Allen, M. D.; Barclay, W. L., Jr.; Ziurys, L. M. The Millimeter and Sub-Millimeter Spectrum of the BaOH Radical. *Chem. Phys. Lett.* **1993**, *205*, 415−422.

(25) Coxon, J. A.; Li, M.; Presunka, P. I. Laser Fluorescence Excitation Spectroscopy of Calcium Monohydroxide and Calcium Monodeuteroxide: the $\tilde{A}^2\Pi-\tilde{X}^2\Sigma^+$ (100)−(000) Band System and the (100)−(020) Fermi Resonance. *J. Mol. Spectrosc.* **1991**, *150*, 33−45.

(26) Fernando, W. T. M. L.; Douay, M.; Bernath, P. F. Vibrational Analysis of the $\tilde{A}^2\Pi-\tilde{X}^2\Sigma^+$ and $\tilde{A}'^2\Pi-\tilde{X}^2\Sigma^+$ Transitions of Barium Hydroxide (BaOH) and Barium Deuteroxide (BaOD). *J. Mol. Spectrosc.* **1990**, *144*, 344−351.

(27) Kramida, A.; Ralchenko, Yu.; Reader, J.; NIST ASD Team *NIST Atomic Spectra Database*, version 5.0. http://physics.nist.gov/asd (2011).

(28) Thompson, C. A.; Andrews, L. Reactions of Laser Ablated Be Atoms with H_2O: Infrared Spectra and Density Functional Calculations of HOBeOH, HBeOH, and HBeOBeH. *J. Phys. Chem.* **1996**, *100*, 12214−12221.

(29) Heaven, M. C.; Bondybey, V. E.; Merritt, J. M.; Kaledin, A. L. The Unique Bonding Characteristics of Beryllium and the Group IIA Metals. *Chem. Phys. Lett.* **2011**, *506*, 1−14.

(30) Yu, S.; Wang, J.-G.; Sheridan, P. M.; Dick, M. J.; Bernath, P. F. Laser Spectroscopy of the $\tilde{A}^2\Pi-\tilde{X}^2\Sigma^+$ 0_0^0 and $\tilde{C}^2\Pi-\tilde{A}^2\Pi$ 0_0^0 Transitions of SrOD. *J. Mol. Spectrosc.* **2006**, *240*, 26−31.

(31) Wang, J. G.; Tandy, J. D.; Bernath, P. F. High-Resolution Laser Excitation Spectroscopy of the $\tilde{A}^2\Pi(000)-\tilde{X}^2\Sigma^+(000)$ Transition of BaOH. *J. Mol. Spectrosc.* **2008**, *252*, 31−36.

(32) Li, M.; Coxon, J. A. High-Resolution Analysis of the Fundamental Bending Vibrations in the $A^2\Pi$ and $X^2\Sigma^+$ States of CaOH and CaOD: Deperturbation of Renner−Teller, Spin−Orbit and K-Type Resonance Interactions. *J. Chem. Phys.* **1995**, *102*, 2663−2674.

(33) Merritt, J. M.; Kaledin, A. L.; Bondybey, V. E.; Heaven, M. C. The Ionization Energy of Be_2, and Spectroscopic Characterization of the (1) $^3\sum_u^+$, (2) $^3\Pi_g$, and (3) $^3\Pi_g$ States. *Phys. Chem. Chem. Phys.* **2008**, *10*, 4006−4013.

(34) Merritt, J. M.; Bondybey, V. E.; Heaven, M. C. Experimental and Theoretical Study of the Electronic Spectrum of BeAl. *Phys. Chem. Chem. Phys.* **2008**, *10*, 5403−5411.

(35) Salami, H.; Ross, A. J. A Molecular Iodine Atlas in ASCII Format. *J. Mol. Spectrosc.* **2005**, *233*, 157−159.

(36) Werner, H.-J.; Knowles, P. J.; Lindh, R.; Manby, F. R.; Schütz, M.; et al. *MOLPRO*, version 2010.1, a package of ab initio programs; Cardiff University: Cardiff, UK, 2010.

(37) Widmark, P. O.; Malmqvist, P.; Roos, B. O. Density Matrix Averaged Atomic Natural Orbital (ANO) Basis Sets for Correlated Molecular Wave Functions. I. First Row Atoms. *Theor. Chim. Acta.* **1990**, *77*, 291−306.

(38) Werner, H. J.; Knowles, P. J. An Efficient Internally Contracted Multiconfiguration-Reference Configuration Interaction Method. *J. Chem. Phys.* **1988**, *89*, 5803−5814.

(39) Knowles, P. J.; Werner, H. J. An Efficient Method for the Evaluation of Coupling Coefficients in Configuration Interaction Calculations. *Chem. Phys. Lett.* **1988**, *145*, 514−522.

(40) Langhoff, S. R.; Davison, E. R. Configuration Interaction Calculations on the Nitrogen Molecule. *Int. J. Quantum Chem.* **1974**, *8*, 61−72.

(41) Berning, A.; Schweizer, M.; Werner, H.-J.; Knowles, P. J.; Palmieri, P. Spin−Orbit Matrix Elements for Internally Contracted Multireference Configuration Interaction Wavefunctions. *Mol. Phys.* **2000**, *98*, 1823−1833.
(42) Kramida, A.; Ralchenko, Yu.; Reader, J.; NIST ASD Team *NIST Atomic Spectra Database*, version 5.1; http://physics.nist.gov/asd (2013).
(43) Jensen, P. Hamiltonians for the Internal Dynamics of Triatomic Molecules. *J. Chem. Soc., Faraday Trans. 2* **1988**, *84*, 1315−1340.
(44) Jensen, P. A New Morse Oscillator-Rigid Bender Internal Dynamics (MORBID) Hamiltonian for Triatomic Molecules. *J. Mol. Spectrosc.* **1988**, *128*, 478−501.
(45) Jensen, P.; Brumm, M.; Kraemer, W. P.; Bunker, P. R. A Treatment of the Renner Effect Using the MORBID Hamiltonian. *J. Mol. Spectrosc.* **1995**, *171*, 31−57.
(46) Jensen, P.; Odaka, T. E.; Kraemer, W. P.; Hirano, T.; Bunker, P. R. The Renner Effect in Triatomic Molecules with Application to CH_2^+, MgNC and NH_2. *Spectrochim. Acta, Part A* **2002**, *58A*, 763−794.
(47) Hirano, T.; Bunker, P. R.; Patchkovskii, S.; Nagashima, U.; Jensen, P. The Predicted Spectrum of FeOH in its Renner-Degenerate X^6A' and A^6A'' Electronic States. *J. Mol. Spectrosc.* **2009**, *256*, 45−52.
(48) Western, C. M. *PGOPHER, A Program for Simulating Rotational Structure*; University of Bristol: Bristol, U.K., 2007.
(49) Tackett, B. S.; Clouthier, D. J. Observation of a New Phosphorus-Containing Reactive Intermediate: Electronic Spectroscopy and Excited-State Dynamics of the HPBr Free Radical. *J. Chem. Phys.* **2005**, *123*, 144304/1−144304/14.
(50) Schlag, E. W. *ZEKE Spectroscopy*; Cambridge University Press: Cambridge, U.K., 1998; p 256.